Project 071 Predictive Simulation of nvPM Emissions in Aircraft Combustors

Georgia Institute of Technology

Project Lead Investigator

Suresh Menon
Professor at the School of Aerospace Engineering
Georgia Institute of Technology
270 Ferst Drive, Atlanta, GA 30332-0150
404-894-9126
suresh.menon@aerospace.gatech.edu

University Participants

Georgia Institute of Technology (GT)

- P.I.: Prof. Suresh Menon
- FAA Award Number: 13-C-AJFE-GIT-067
- Period of Performance: October 1, 2022 to September 30, 2023
- Tasks:
    1. Kinetic modeling: improvement in soot kinetic models and chemistry of jet fuels under rich quench-lean (RQL) combustor operating conditions
    2. Nucleation modeling: predicting incipient particle nucleation rates according to polycyclic aromatic hydrocarbon (PAH) dimerization rates from molecular dynamics (MD) simulations
    3. Surface growth and aggregation modeling: reaction-transport-limited growth of soot particle models for cluster–cluster aggregation
    4. Large eddy simulation (LES) of multiphase reacting physics inside an RQL combustor

Project Funding Level

The current FAA funding is for a 3-year effort (July 2020 to September 2023), with a request of $500,000 per year from ASCENT (per year). An additional request for a no-cost extension has been submitted. Cost-sharing is provided as follows.

- GT provides cost-sharing for its share of $150,000 per year. The GT point of contact is Kevin Ellis (kevin.ellis@aerospace.gatech.edu).
- Raytheon Technologies Research Center (RTRC) provides cost-sharing of $250,000 per year. Dr. Colket is a consultant on this project with many years of experience in soot modeling. The RTRC contact is John LaSpada (LaSpadJW@RTRC.utc.com).
- The University of Michigan (UM) provides cost-sharing in the amount of $100,000 per year. The UM point of contact is Alexandra Thebaud (thealexi@umich.edu).
  A no-cost extension until September 2024 has been granted.

Investigation Team

GT

Prof. Suresh Menon, GT: (P.I.), Task 4
Mr. Shubham Karpe, GT: (Student), Task 4

RTRC

Dr. Miad Yazdani, (co-P.I.), Task 3
Dr. Steve Zeppieri, (co-P.I.), Task 1
Dr. Meredith Colket, (co-investigator), Task 1

UM

Prof. Angela Violi, (co-P.I.), Task 2
Mr. Jacob Saldinger, (Student), Task 2

Project Overview

This project is being used to establish a new multiscale approach to predict soot formation in aircraft combustors. A hierarchy of first-principles simulation methods is being used to account for the multiscale physics of the formation and transport of non-volatile particulate matter (nvPM, also called soot in the literature). The final objective is to use this multiscale approach to model the physics in LES of realistic gas turbine combustors. We target and isolate the layers of empiricism that currently exist, for example, in particle inception models, the roles of precursor species in nucleation, the particle shape assumptions and their impact on surface growth, the sensitivity of predictions to particle size distribution, and the ad hoc coagulation/coalescence mechanisms. The team already has all modeling tools, but a systematic coupling of these tools in a multiscale, multiphysics strategy has yet to be accomplished by any research group. Hence, this study will establish new predictive ability by integrating these capabilities.

The multiscale and multiphysics layers of collaborations among the cost-sharing groups are summarized in Figures 1 and 2, and briefly described herein. The kinetics group at RTRC is conducting a study to understand the role of gas-phase kinetics in predicting important species potentially labeled as soot precursors. The information on reduced kinetics from RTRC is being used by GT and UM to evaluate LES performance and the process of nucleation. In the UM study, the propensity of gas-phase species to form dimers (considered the building blocks of soot inception) under flame conditions is being studied. Identification of soot precursors and the rates of formation of soot nuclei will be the output from these studies. This nucleation rate will be provided to GT to update the source terms associated with nucleation processes through a six-moment method of moment with interpolative coefficients (6-MOMIC) approach, and the information on the structures of these soot nuclei will be provided to RTRC for modeling of surface growth and aggregation processes. Outputs from the aggregation studies in RTRC in the form of global surface growth and aggregation models will then be fed back to GT to update the source-term surface growth and aggregation models in the 6-MOMIC approach. Canonical studies are underway at GT to provide information regarding the variations in local conditions, such as pressure, temperature, and local equivalence ratios due to turbulence–chemistry interactions; this information should be useful in each stage of the abovementioned studies. LES studies at GT will also involve modeling the effects of chemistry–soot–turbulence interactions by using advanced subgrid models including the linear eddy mixing (LEM) model. As a project deliverable (at the end of this research effort), the final assessment of both the existing soot model and the improved soot model will be conducted in canonical flame configurations.

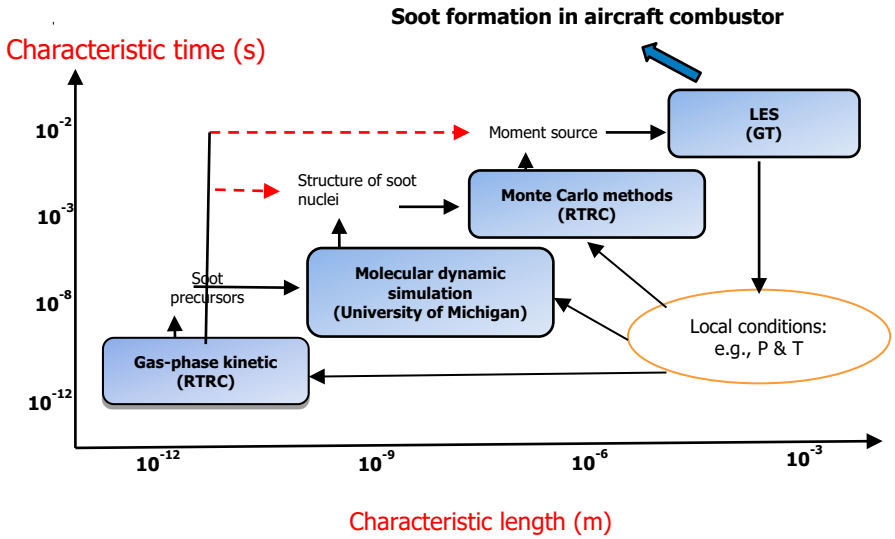

Figure 1. Multiscale collaborative efforts to improve nvPM (soot) predictions.

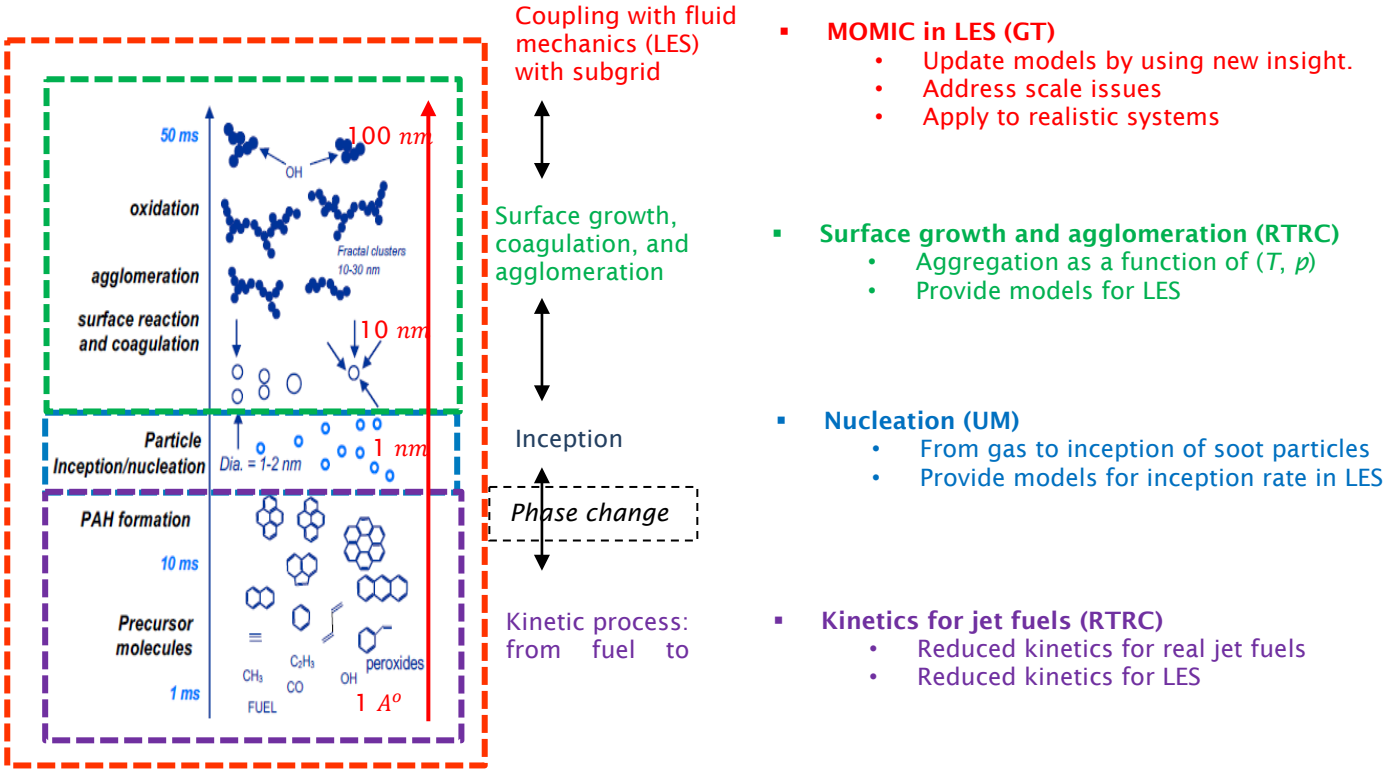

Figure 2. Multiscale collaborative efforts to improve nvPM (soot) predictions.

Task 1 – Kinetic Modeling

RTRC

Objective

The objective of this task is to develop validated, detailed, and reduced chemical kinetic models of parent fuel decomposition and oxidation reactions, with a special focus on fuel rich chemistry, to enable the accurate evolution of PAH/soot precursor formation and incipient soot particle formation, and the evaluation and improvement of reduced-order soot formation models. Year 1 fuel activities focused on ethene, whereas Year 2 efforts shifted the focus to Jet A fuels. In Year 3, efforts continued toward optimizing fuel chemistry as well as soot kinetics at RQL-relevant conditions.

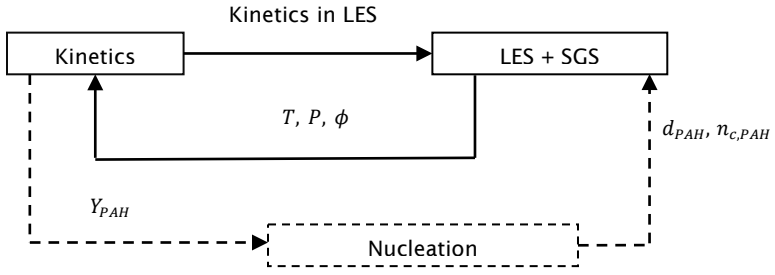

Figure 3. Coupling of LES–kinetic activities.

Research Approach

Reduced-order model development for use in LES of RQL combustors

The schematic in Figure 3 shows the coupling among the LES, nucleation, and kinetic activities focused on during the current Year 3 of the project, where T, P, and ϕ represent the temperature, pressure, and equivalence ratio of the surrounding gas phase, respectively. The LES studies at GT are being conducted at T_{in} = 600 K and P = 5.8 atm. These conditions are used herein for optimization of chemistry for jet fuels as well as soot kinetic model optimization for the range of ϕ. Moreover, PAH represents the polycyclic aromatic hydrocarbon species considered the soot precursors. The objective of the current kinetic efforts was focused on downselecting the detailed kinetic model of jet fuels and reducing it to a non-stiff version with finite rate expressions for production of precursor species determining Y_{PAH}. This kinetic model is to be fed directly into LES studies at GT. The precursor species characteristics (n_{PAH}, d_{PAH}) and concentrations will also be input into nucleation studies at UM to assess their ability to form dimers.

In Year 1, ethene kinetics with varying details of PAH/particulate matter (PM)-related chemistry were assessed. Given that the ultimate goal of this effort is the development of chemical kinetic models coupled to PAH and soot (PM) formation for both logistic (Jet A) and alternative fuels, we investigated four detailed mechanisms. We used the HyChem method, in which semi-empirical reactions treat the parent fuel decomposition process to the relevant intermediate hydrocarbon species, and the so-called SERDP technique, in which compositions of several surrogate hydrocarbon species are formulated that capture the bulk properties of the fuel of interest. (For example, Jet A would be considered a binary blend of *n*-dodecane and *m*-xylene.) The HyChem model was coupled with both the SERDP and KAUST PAH-chemistry models for analysis, and the SERDP model was coupled with the SERDP PAH-chemistry model. Finally, the Caltech-mech model was appended with the HyChem model to incorporate additional reactions related to decomposition of Jet A fuels. In the most recent prior annual efforts, comparisons were drawn by using HyChem-KAUST and HyChem-SERDP approaches against the Wang-Frenklach (WF) (Wang, 1997) chemistry, by using the benchmark data for soot formation from ethene fuels. In the current effort, we have incorporated one more detailed mechanism, Caltech-mech. We also used the Pitsch mechanism (Langer, 2023), which is relatively new, for the initial assessment of gas-phase chemistries.

The overall layout of the workflow implemented in this quarterly effort is highlighted in Figure 4.

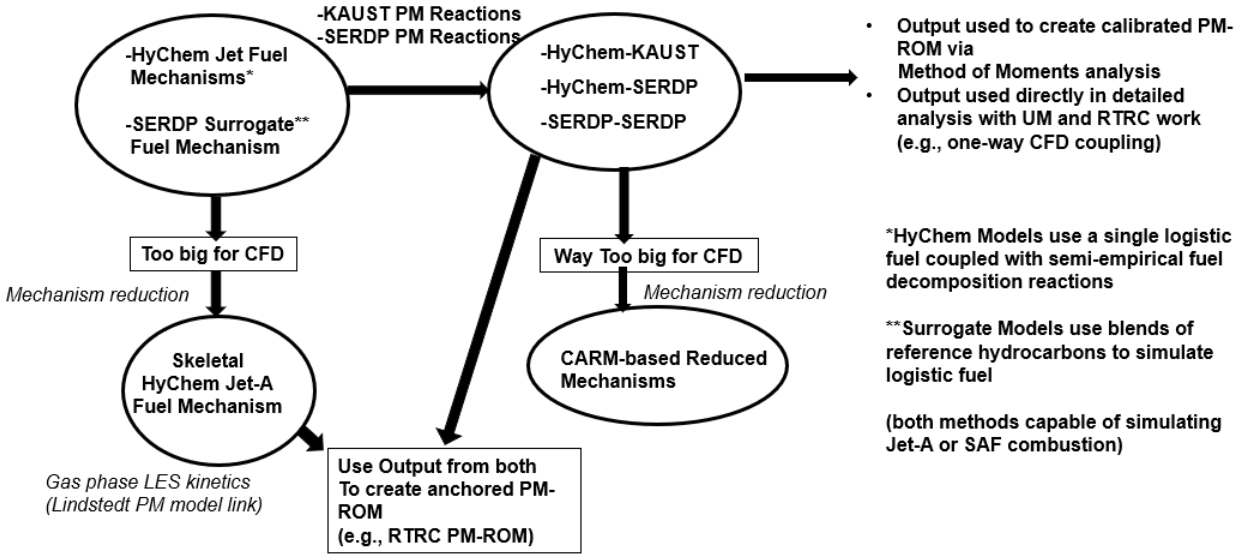

Figure 4. Specific workflow of kinetic activities for jet fuels.

In the first task, overall comparisons of two key species influencing soot formation and growth (C_2H_2 and C_6H_6) among all four kinetic models (HyChem-SERDP, HyChem-KAUST, Caltech-mech, and Pitsch detailed mechanism) is performed for range of equivalence ratios as well as reactor temperatures. The exact Perfectly Stirred Reactor (PSR) conditions are Jet A/air (or 77% nC12, 23% *m*-xylene*), P: 1 atm, τ_{res}: 25 msec, ϕ : 1.9–2.5, T: 1400–2000 K).

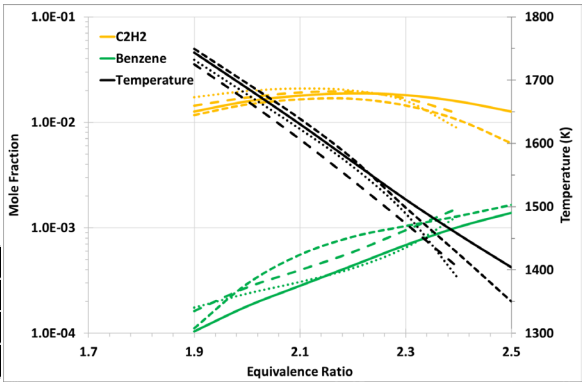

Solid:	**Caltech Mech**
Dash:	**Pitsch et al.**
Dot:	**Hychem/Kaust Mech.**
Long Dash:	**Hychem/SERDP Mech.**

Figure 5. Comparison of C_2H_2, C_6H_6 and temperatures among mechanisms.

Figure 5 suggests that overall predictions of temperature are similar for all mechanisms. Some visible differences arise in the range of higher equivalence ratios. The benzene (C_6H_6) profiles and acetylene (C_2H_2) profiles are in qualitative agreement among mechanisms except the Pitsch mechanism, which must be investigated further. Encouragingly, both HyChem models and the Caltech-mech model have overall satisfactory agreement.

The nucleation studies at UM suggest the roles of heavier PAH species in forming incipient soot particles. Consequently, assessment is conducted to compare predictions of heavier PAH species, such as naphthalene ($C_{10}H_8$), fluorene ($C_{13}H_{10}$), and pyrene ($C_{16}H_{10}$), at the same conditions as above for all four mechanisms. The results from this analysis (Figure 6) suggest a wider spread of PAH species among all four mechanisms that may be crucial in predicting the early nucleation stages of soot formation in large-scale simulations.

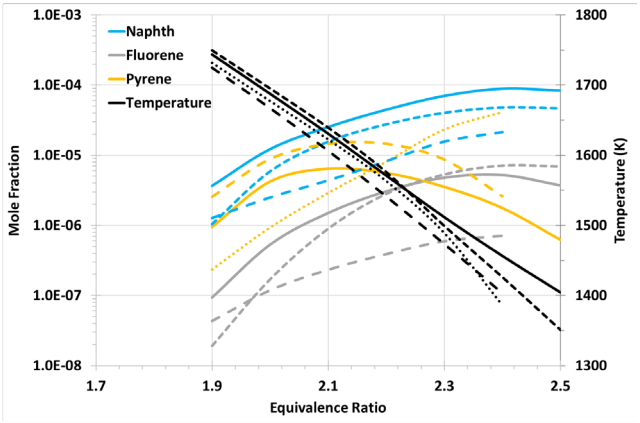

Figure 6. Comparison of heavier PAH species among mechanisms.

The Pitsch mechanism is relatively new and requires further assessment, and hence is not used in later analysis. Further analysis is presented herein for comparing predictions of soot formation for ethene by using WF (demonstrated in previous annual efforts), HyChem-KAUST, HyChem-SERDP, and Caltech-mech with a reduced POM model (optimized rates for the Lindstedt soot model) have been described in earlier annual efforts. Briefly, the PM-ROM is based on the well-known Lindstedt two-equation soot model. The two equations are used to determine the soot mass and soot concentration generated in the system. The necessary rates for model closure are particulate inception/nucleation, particulate surface growth, surface oxidation, and particle coagulation. In the original Lindstedt model, the key PM-forming species is acetylene, molecular oxygen is the key soot oxidation species, and a single Arrhenius rate expression is used for each step. The RTRC formulation extends the original premise by adding benzene as key PM-forming species and the hydroxyl radical as another oxidation species, and by using a double Arrhenius rate expression for both the inception and surface

growth processes, thus enabling the model to capture the well-known and experimentally observed "soot bell" concentration profile with respect to temperature. The results are presented in Figure 7.

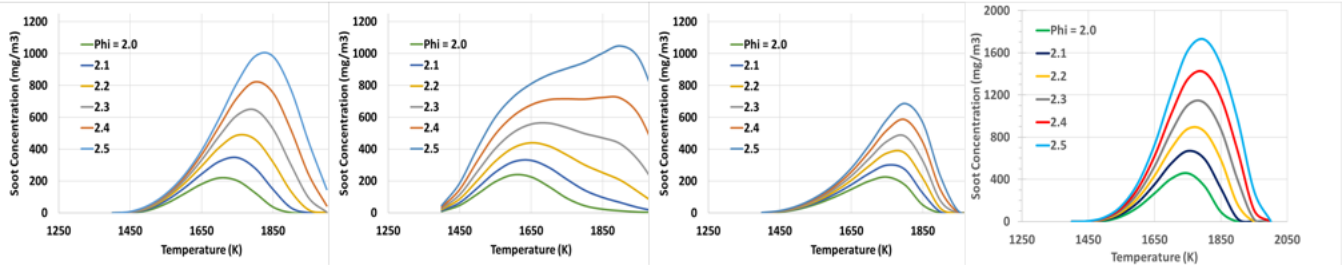

Figure 7. Comparison of soot volume fractions for various gas-phase mechanisms: WF, HyChem-KAUST, HyChem-SERDP, and Caltech-mech from left to right.

Figure 7 suggests that the soot concentration levels at the range of temperature from WF, HyChem SERDP, and Caltech-mech show similar behavior in terms of a bell-shaped dependency on temperature. The HyChem-KAUST predictions are qualitatively very different from those of the other three mechanisms. In quantitative analysis, the HyChem-SERDP mechanism underpredicts soot levels by a factor of 1.5 at higher equivalence ratios than the WF mechanism. Similarly, Caltech-mech overpredicts soot levels by a factor of 1.5–2 with respect to the WF mechanism.

In the next set of activities, predictions are compared by changing the fuel to Jet A fuels under the same operating conditions investigated for ethene fuels described above. The HyChem-KAUST, HyChem-SERDP, and Caltech-mech mechanisms are compared. As shown in Figure 8, the predictions from Caltech-mech and HyChem-KAUST agree with each other quantitatively. However, HyChem-KAUST predicts two peaks in soot levels, whereas Caltech-mech predicts only one peak and a bell-shaped dependency. This qualitative bell-shaped one peak trend is also visible in the predictions of HyChem-SERDP; however, the quantitative magnitude is factor of 3 lower than those of the Caltech-mech and HyChem-KAUST mechanism.

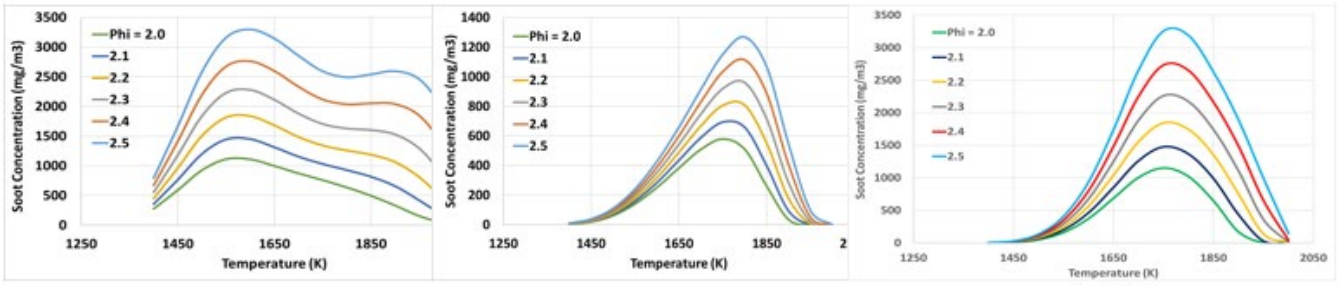

Figure 8. Comparison of soot volume fractions for different gas-phase mechanisms: HyChem-KAUST, HyChem-SERDP, and Caltech-mech, from left to right.

Analysis of the ethene/air and Jet A/air simulations combined for the same reactor conditions, considering the trends as well as quantitative levels of soot predictions, suggests that Caltech-mech appears to be the best mechanism to proceed with performing reductions in the next quarterly efforts.

One of the goals of this effort is the development of a reduced-order model capable of capturing soot formation with liquid fuels, for use in computational fluid dynamics (CFD) applications. The HyChem-SERDP kinetic data were used to benchmark/modify the PM-ROM RTRC previously created for ethene/air systems in the most recent prior quarterly effort. The RTRC model was shown to capture the parabolic shaped concentration profiles (i.e., a soot bell profile) associated with both experimental and detailed analytical models. The above analysis suggested the need to replace the Hychem-SERDP model with the Caltech-mech mechanism; therefore, the latter was the target for the remainder of the annual efforts.

After having assessed the details of PAH based detailed kinetics at range of conditions, we attempted to extend the concepts used to generate a higher fidelity PM-ROM model for use in RQL CFD studies. A numerical shooting fitting procedure was used to establish rate coefficients that enabled the PM-ROM model to identically match the soot concentration levels generated via detailed kinetic analysis coupled with Method of Moments (MoM) soot calculations. In the most recently developed PM-ROM, the reduced model was calibrated against PSR calculations at the elevated pressure (5.8 atm) and air temperature (600 K) conditions of RQL combustor operation. The nominal reactor residence time for these calculations was 5 ms, and the fuel-air equivalence ratio spanned from 1.8 to 2.5. The detailed mechanism used was the previously discussed HyChem-Caltech mechanism.

In the new model method, the double Arrhenius rate expressions are replaced by the numerically optimized rate expressions. These rate values are functions of both temperature and the equivalence ratio. The agreement between the soot concentrations generated via detailed kinetics and MoM and the PM-ROM are shown in Figure 9, indicating quite good agreement.

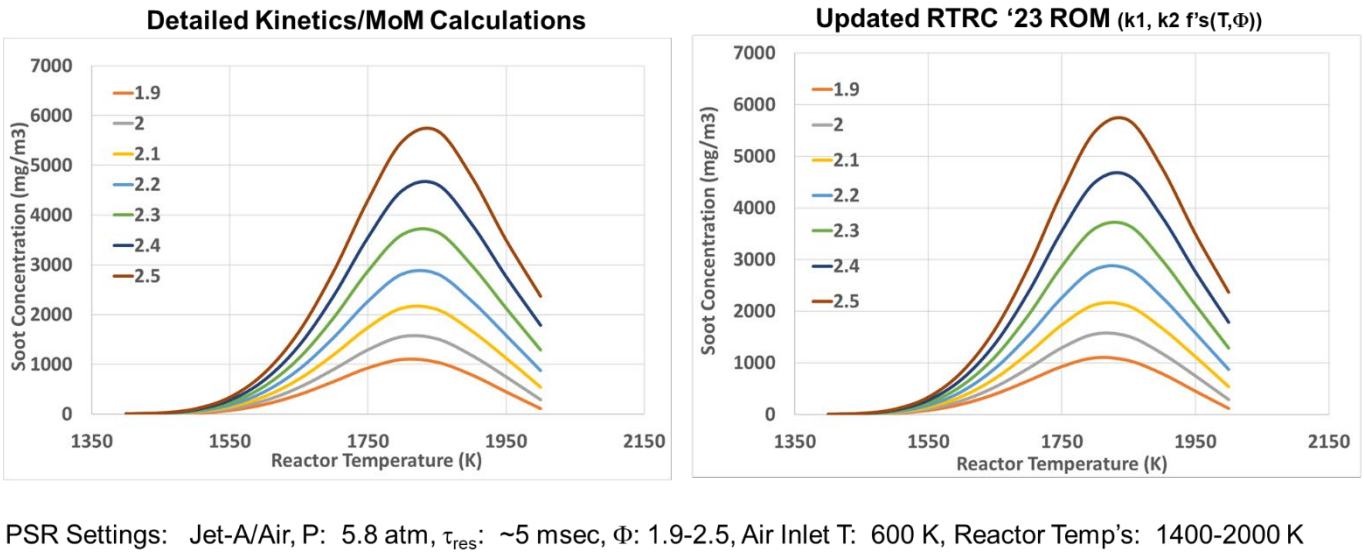

Figure 9. Comparison of soot concentrations generated from the two modeling approaches listed at nominal RQL combustor conditions.

Given that two-dimensional (i.e., temperature and equivalence ratio) correlation might not be computationally efficient, the developed rate correlations were reduced to one dimension as follows. The developed rate expression equivalence ratio dependencies were averaged over the range, and yielded rate constants that were functions of only temperature. The average rate expressions for nucleation and surface growth processes are shown in Figure 10.

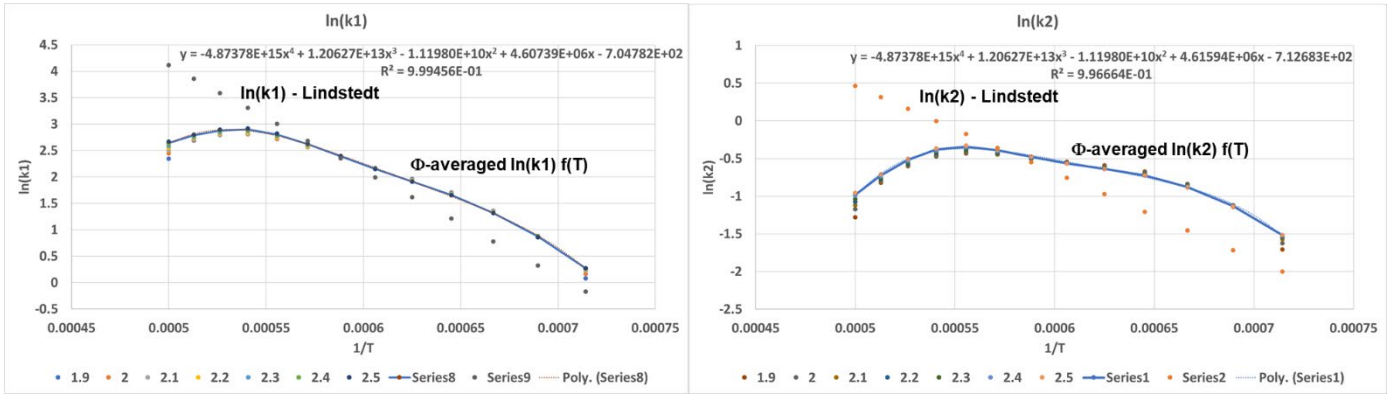

Figure 10. Fuel-air mixture averaged kinetic rate expressions for nucleation (left) and surface growth (right) for use in the PM-ROM tool for the RQL CFD analysis.

With this new temperature-only rate expression, the soot concentration outputs associated with the PSR simulations were then computed and compared against the original detailed chemistry/MoM calculations. This comparison is shown in Figure 11. A slight decrease and slight increase are observed in the fuel rich and lean conditions, respectively, but overall, the concentration values are in good agreement with the detailed data. These final expressions will be incorporated into the PM-ROM that will be used by the GT team in conjunction with the CFD analysis.

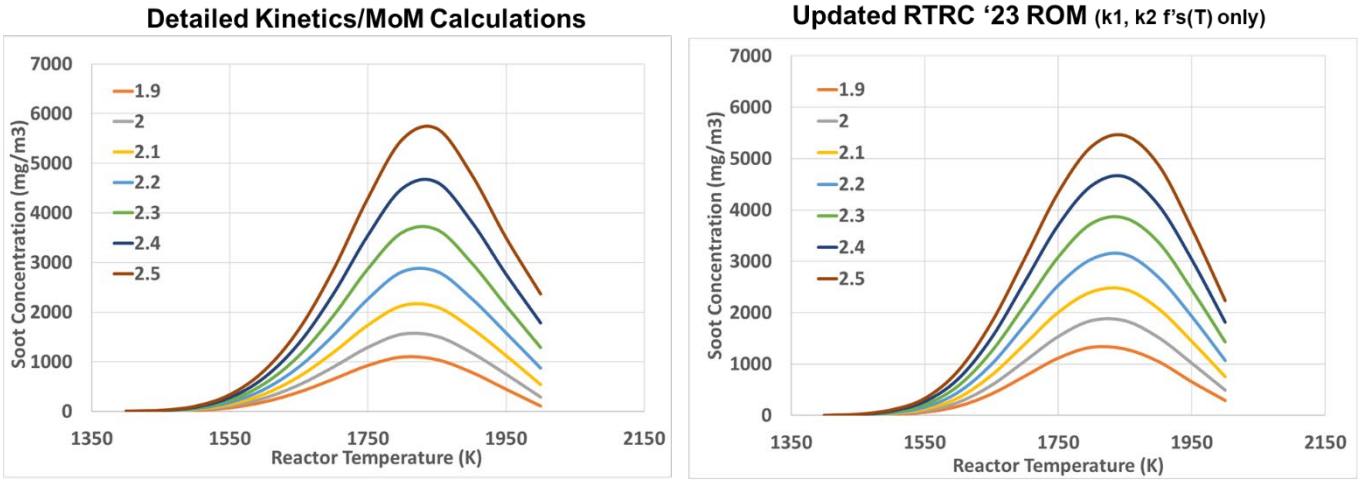

Figure 11. Comparison of soot concentrations generated from the two modeling approaches listed at nominal RQL combustor conditions.

The goal of this year's activities was to determine whether a suitably compact mechanism that incorporates both Jet A and PAH/PM kinetic information could be developed. From the analysis conducted to date, the detailed mechanism has been constructed, and the PM-ROM has also been optimized to match its predictions with a detailed MOM model. The reduced chemistry and the PAH based ROM model will be used by GT for CFD analysis of an RQL combustor, which are being provided.

Milestone
Detailed Jet A fuel chemistry, its reduction for use in CFD analysis, and optimization of the PM-ROM model is planned for 9/30/2024.

Major Accomplishments
Reduced Jet A fuel chemistry and optimized PM ROM at RQL-relevant conditions.

Publications
None.

Outreach Efforts
None.

Awards
None.

Student Involvement
None.

Plans for Next Period
Future efforts will focus on providing these inputs regarding reduced kinetics and the PM-ROM model to GT for CFD simulations of an RQL combustor.

Task 2 – Nucleation Modeling
UM

Objective
The objective of this task is to develop models for nanoparticle inception, a critical step in predicting emissions. This effort bridges the work on gas-phase chemistry (RTRC) with the model for particle growth (RTRC), and provides inputs for the MOMIC model (GT) and growth models (RTRC) using atomistic simulations.

Research Approach
Current models for particle inception are unable to reproduce a variety of experimental data, including molecular structure. This work is aimed at developing a predictive model for particle inception that can provide accurate chemical and physical growth pathways for PAHs. MD simulations are used to study the collisions of PAHs and the formation of aromatic dimers leading to soot inception.

In the most recent annual efforts, methods and the MD approach were established for the assessment of the dimer formation stability of different aromatic species. We performed atomistic simulations of these species and higher PAH species, also including oxygen content. Figure 12 shows the structures of gas-phase compounds considered in this study and the results for their homo-dimerization propensity. The data points are broadly clustered in three groups. The first is composed of the compounds I.C. (462 u), I.D. (462 u), and I.E. (460 u), which have the same mass and oxygen/carbon ratios (0.125) and are less stable than I.A. (448 u) and I.B. (472 u), which constitute the second group. This difference indicates that the presence of oxygen slightly destabilizes the dimers, an effect possibly caused by the greater repulsive electrostatic interactions of oxygenated molecules than observed for pure aromatic hydrocarbons. The third group is formed by I.F. (402 u), I.G. (452 u), and I.H. (502 u), which are less likely to dimerize than the other two groups. The low dimer stability of the third group might be due to the presence of a sigma bond, which introduces an internal rotatable bond that interferes with the formation of clusters. Several conclusions were drawn from this study. First, the details of the structures of the species that nucleate cannot be ignored. Mounting evidence indicates that the presence of five-membered rings, aliphatic side chains, and oxygenated groups in soot precursors does not change the nucleation mechanism leading to soot formation. Our results pertaining to both the dimerization propensity and the change in free-energy barriers between monomers and dimers, both of which directly relate to the kinetic rates of dimerization, suggest otherwise. Second, the effects of shape, the presence of oxygen, mass, and rotatable bonds are tightly intertwined, and have differing

importance as well as diverse temperature dependencies, although they are all dominated by entropic effects at high temperatures. The presence of oxygen affects the dimer propensity by decreasing the molecular cohesion due to electrostatic repulsion; however, notably, the force field used in this study cannot capture the effect of molecular polarizability.

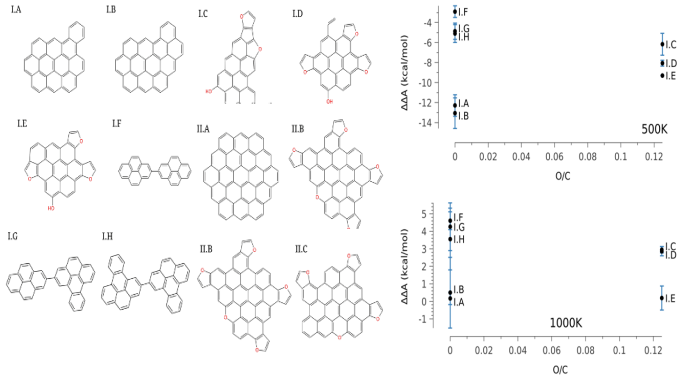

Figure 12. Structural formula of gas-phase compounds (left) and homo-dimerization propensity at 500 K and 1000 K, as a function of the oxygen/carbon ratio.

These results have been used as a first approach toward the development of predictive trends for quantifying dimer stability. Because of the presence of various intertwined dependencies, we will need a new approach to separate the contributions and their relative importance. In the next efforts, MD simulations with machine learning approaches to identify the main characteristics that drive nucleation and determine the corresponding rates are discussed.

In the next task, we have focused on machine learning algorithms, with the goal of leveraging this technique to predict the dimerization propensity of various PACs. Although molecular dynamics simulations can provide this information for specific dimer pairs, extending simulations to all potential dimer components is not feasible. With millions of different PACs observed in even simple flame, computing this information for all possible PACs would be excessively costly, particularly when accounting for the combinations of heterodimerization among PAC molecules. Recently, machine learning has shown potential to learn complex quantitative relationships among PAC properties and predict the energy difference between the monomeric and dimeric state for an arbitrary pair of PACs, with minimal computational cost. However, the approach considers only thermodynamic energy differences at a single temperature and therefore is insufficient to predict the energy barriers needed to derive kinetic rates.

As a first step, we perform numerous Meta dynamics molecular dynamics simulations to calculate the dimer energy barrier for a large dataset of PACs at multiple temperatures. This value is critical in characterizing the kinetic stability of the PAC dimer, and, in conjunction with equilibrium data, can provide a comprehensive description of forward and reverse barriers and rates in the dimerization process. MD simulations enhanced by Meta dynamics were used to reproduce the free-energy landscape of the dimerization process as a function of the center-of-mass distance. To define the chemical space, we considered a wide set of PACs, as reported in the most recent report, which broadly reproduces the sizes, shapes, and functional groups observed in flame systems. To describe PAC chemistry, we compute a set of 312 descriptors for each molecule. These descriptors capture properties such as mass, atomic ratios such as carbon-hydrogen ratio, and counts of specific subgroups such as aromatic rings. From our simulations, we obtain 315 unique energy barriers between the monomer and dimer states. Generally, we observe the same qualitative relationships with size and temperature. All other parameters being constant, free-energy barriers tend to increase with mass as Van der Waal's and electrostatic interactions become stronger and decrease with temperature as entropic effects increase in importance. importantly, however, these two parameters are insufficient to describe all differences observed in the energy barrier, and a quantitative trend cannot accurately be derived solely from these two values. We have started to investigate machine learning algorithms, and we are currently implementing such an approach while still running MD simulations. Figure 13 shows our target machine learning algorithm.

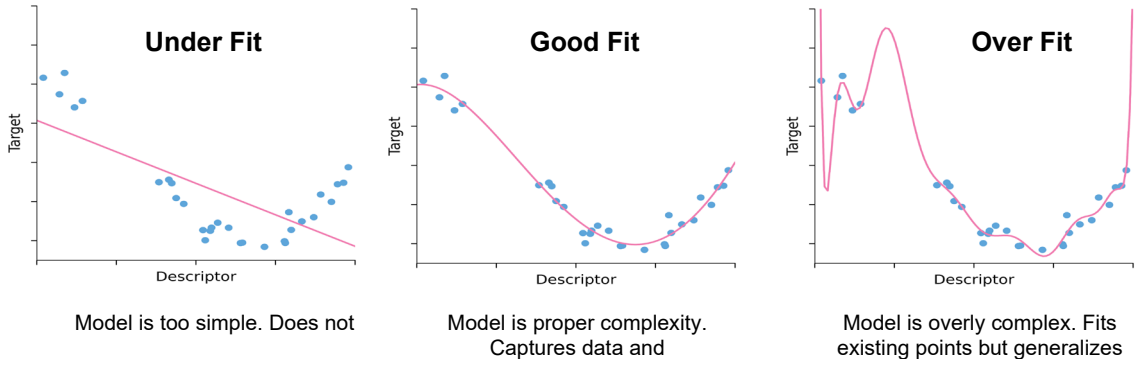

Figure 13. Evaluation of machine learning algorithms.

To analyze the complex space, we used machine learning with a model with good fit. Before training our machine learning model, we eliminated similar features by removing any feature with a variance of zero and any feature with a Pearson correlation greater than 0.95. To build a predictive model for the Feature Extraction (FE) of aggregation, we applied the Lasso method, because it has high accuracy and often enables interpretable predictions. Lasso is a supervised machine learning regression model that minimizes a loss function and uses the least absolute shrinkage and selection operator. This model has been successfully applied to make interpretable predictions in chemical problems, because it eliminates extraneous features and selects only a subset of properties needed to make the predictions.

Our model outperforms existing physical dimerization models described in the literature. We compared our results, including the test on a restricted dataset with no data leakage, with three additional models. One advantage of Lasso is its ability to provide a degree of interpretability regarding the aspects that control the prediction, because it sets the coefficients of unused features to zero. Thus, by analyzing which features the Lasso model retains, we can gain a sense of which molecular properties are important for predicting the FE of dimer aggregation. Of note, whereas some of the molecular properties discussed below resemble quantities that have been used in the past to predict the aggregation propensity, they are not generally interchangeable with those in the literature. Overall, across all 105-fold cross-validations, the model selects a nearly identical set of 10 features. If we exclude these top features, no other features are selected in more than four folds and therefore are not discussed. Broadly, the top features can be divided into three groups of properties that are important for PAC dimerization: size, shape, and presence of specific chemical groups.

The first class of properties comprises extrinsic properties that are broadly related to the size of the molecule. Specifically, the algorithm selected the number of aromatic rings, the number of carbons not connected to a hydrogen, the number of tessellations containing four carbons, the number of tessellations with three carbons and a hydrogen, and the number of six-membered rings. Figure 14 shows that the FE of dimerization is strongly associated with the (harmonic) average number of aromatic rings in the dimer (Pearson coefficient of −0.8397 and Spearman coefficient of 0.8719). This result agrees with the general observation that PACs often cluster in lateral stacks, and the interaction strength among PACs is closely associated with their number of aromatic rings. Among the molecular descriptors in this class, the number of aromatic rings is the feature with the highest correlation with the FE (more than the number of six-membered rings, for example), but crucially by itself it is not sufficient to fully capture the physical dimerization. A linear fit of the FE as a function of the total number of aromatic rings produces a prediction model with an root mean square error (RMSE) of 15.6 kJ mol^{-1} and a mean absolute error (MAE) of 11.3 kJ mol^{-1}, which has a significantly larger error than our model and is (not coincidentally) comparable to using only the mass as a descriptor. Some features in this group encode size with molecular shape information. One such example is the number of internal carbon atoms, defined as the aromatic carbon atoms that are not bonded to H atoms. Because most of the molecules in the dataset are highly pericondensed hydrocarbons, these PACs will have a greater percentage of internal carbons than catacondensed PACs.

In recent efforts, we closely collaborated with RTRC kinetics to identify PAH species available in the gas-phase mechanism. We are using a machine learning algorithm to predict energy barriers and eventually rates at RQL-relevant operating

conditions for identifying the rates of dimers causing inception of soot species; these efforts will be provided as input to the RTRC surface growth group.

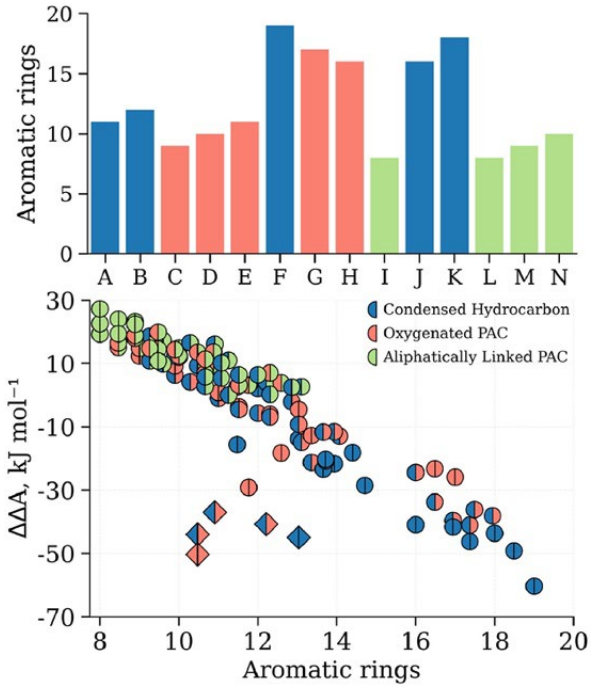

Figure 14. Relationship between the number of aromatic rings and dimerization FE. Top: number of aromatic rings associated with each dimer. Bottom: aggregation propensity compared with the average number of aromatic rings in the dimer.

Milestone
Establishing a machine learning approach to assess a large pool of PAH species at RQL-relevant conditions is planned for 9/30/2024.

Major Accomplishments
Established machine learning-based MD predictions for nucleation rates due to PAH dimerization.

Publications
None.

Outreach Efforts
None.

Awards
None.

Student Involvement
One student at UM is involved in this work.

Plans for Next Period

In future efforts, we seek to provide inputs from machine learning algorithm predictions of energy barriers and eventually nucleation rates at RQL-relevant operating conditions. These rates will be provided as input to the RTRC surface growth group.

Task 3 – Surface Growth and Aggregation Modeling

RTRC

Objective

The objective of this task is to develop a physics-based framework for the prediction of soot particle growth after the inception process. The growth consists of agglomeration due to collisions between the primary particles and surface growth because of direct deposition of the precursors on the aggregate. The final aggregate fractal structure and its temporal evolution as a function of local conditions are of interest. This model will provide the morphology characteristics and the growth rate of the particles, which will serve as inputs into the MOMIC formulation.

Research Approach

Soot particles from nucleation stages undergo various surface growth processes and form primary particles. These primary particles are spherical and typically have diameters of 1–10 nm. The focus of this effort is to understand the evolution of the fractal dimension of aggregates from the formation of primary particles to final fractal aggregates, through processes of surface growth and aggregation. Experimentally, the structures of these soot particles have been demonstrated to be dependent on the local conditions (e.g., the local equivalence ratio). These surface growth processes can occur because of heterogeneous reactions of gas-phase precursors on solid soot particle surfaces (reaction-limited growth) or through the transport of soot precursors in high-speed flames (transport-limited growth). Most of the current growth models account for only reaction-limited growth and ignore transport-limited growth as well as cluster–cluster interactions, which may be important in aggregate formation. In this work, information on background gas-phase species contributing to soot particles, the structure of the initial soot nuclei, and the local conditions is merged to understand the fundamental processes contributing to the formation of large soot aggregates.

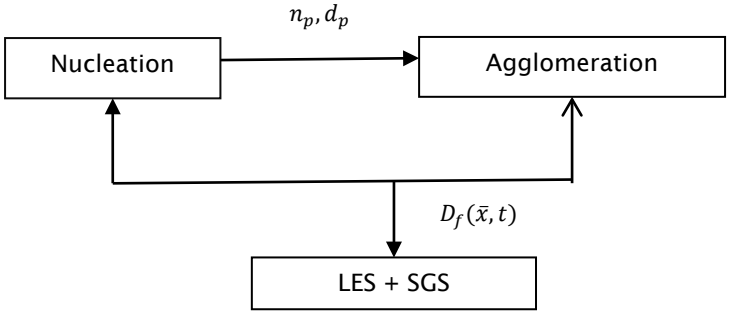

Figure 15. Post-inception growth of soot particles (LES–RTRC–UM coupling).

The coupling of the growth framework being developed at RTRC with MD simulations from UM and the LES study at GT is briefly highlighted in Figure 15. The growth module takes the number density and size distribution of incipient soot particles from nucleation as an input, then tracks the growth of such particles along the statistically averaged path lines, which have varying background LES conditions in the form of temperature (*T*), pressure (*P*), and local equivalence ratio (ϕ), as detailed below. The output from such studies in the form of the parametrized fractal dimension (D_f) will be fed back into the LES–MOMIC soot approach.

The developed post-inception growth model described in the previous annual effort has been shown to capture the effects of different operating conditions on the growth characteristics of the particles, including size and morphology. However, the parametric exercise of this model could become computationally prohibitive with a sweep over a range of operating parameters and combinations therein. A path line-sampling approach was proposed (schematic in Figure 16), wherein the full flow-field (obtained by the LES) is represented by statically sampled path lines, over which the operating conditions are

time variant. For example, the temperature and fuel/air ratio evolve over the course of time as a particle moves from the injector toward the exit of the combustor. This time history is then provided to the growth model, and the variation in particle characteristics is solved over the course of this timeframe for each individual path-line histogram (example output shown in Figure 17). This information is then fed back into the LES with time–space mapping through the path-line coordinates and nearest-point interpolation, to provide a full spatial representation of growth information, which is then used in the MOMIC approach. This approach effectively reduces the computational overhead of the growth model to a dozen simulations (on the basis of the assumption that this number of path lines is sufficient to properly sample the combustor flow field), in contrast to potentially hundreds with the conventional parametric approach. Of note, in this one-way coupling approach, the macroscopic changes in the flow-field due to the interaction with the soot-particle transport are assumed to have negligible effects on the growth characteristics of the particles.

The post-inception growth modeling framework and the coupling therein to the LES framework is demonstrated for the solution of NASA-LDI geometry. The information along statistically sampled path lines is provided to the post-inception model, which then solves the evolution of the soot clusters along those path lines. To obtain a sense of primary particle size and number density, a classical nucleation theory is used, which takes the following form.

$$N_0(t) = [M(t)] \exp\left(-\frac{\Delta G_0(t)}{kT}\right)$$

Notably, this formulation, or terms therein, will eventually be replaced by the solution of the MD simulation. An example of primary particle number density along one of the path lines in the rig is shown in Figure 18. Figure 19 shows the evolution of soot particle characteristics (fractal dimension and average size) along two of the path lines inside the combustor.

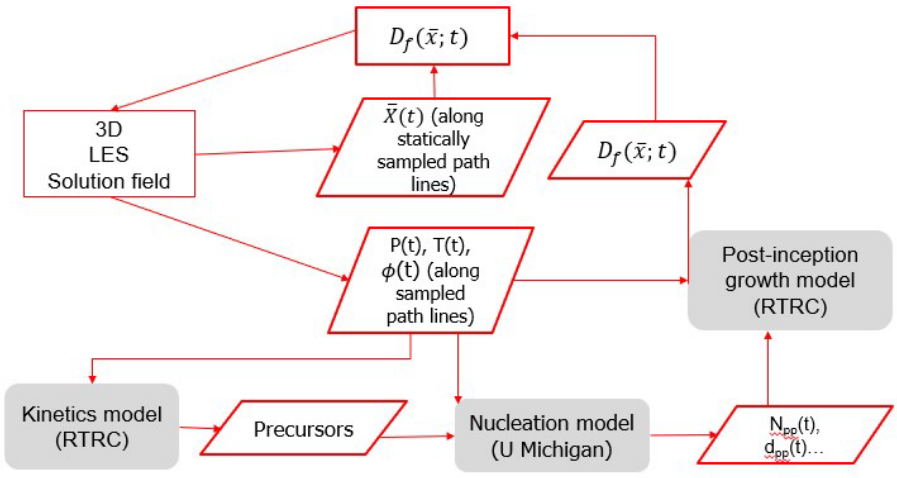

Figure 16. One-way coupled strategy for growth of soot particles.

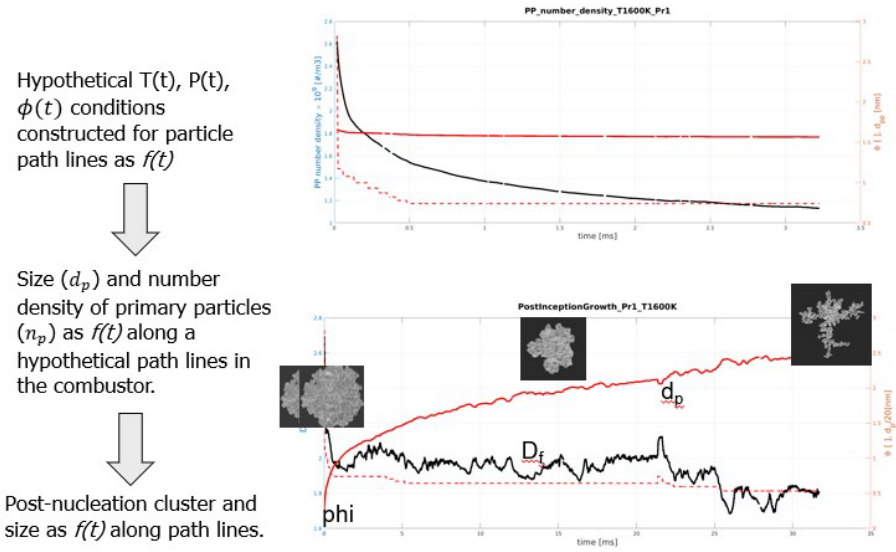

Figure 17. Demonstration of a one-way coupled strategy along a hypothetical LES path line.

The demonstration with the NASA-LDI combustor has provided confidence in using the framework for the RQL combustor (described later in the LES section). We are in the process of translating similar path-line data for the RQL combustor at the relevant conditions and using the nucleation rates provided by the MD framework described in the earlier section to predict the soot evolution along the path lines at these realistic combustor operating conditions. Further analysis will be conducted to understand the growth of fractals along other statistical path lines, to reveal how the primary particles grow and how they form fractals to parametrize this growth as a function of particle sizes. The current MOMIC model in GT LES has two sensitive parameters for post-inception growth: (a) the critical diameter to which particles grow and form spherical particles through coalescence and b) the fractal dimension dictating the fractal growth of soot primary particles. The Monte Carlo (MC) simulations will be assessed against the growth models of GT LES code to determine whether some of these criteria are justified.

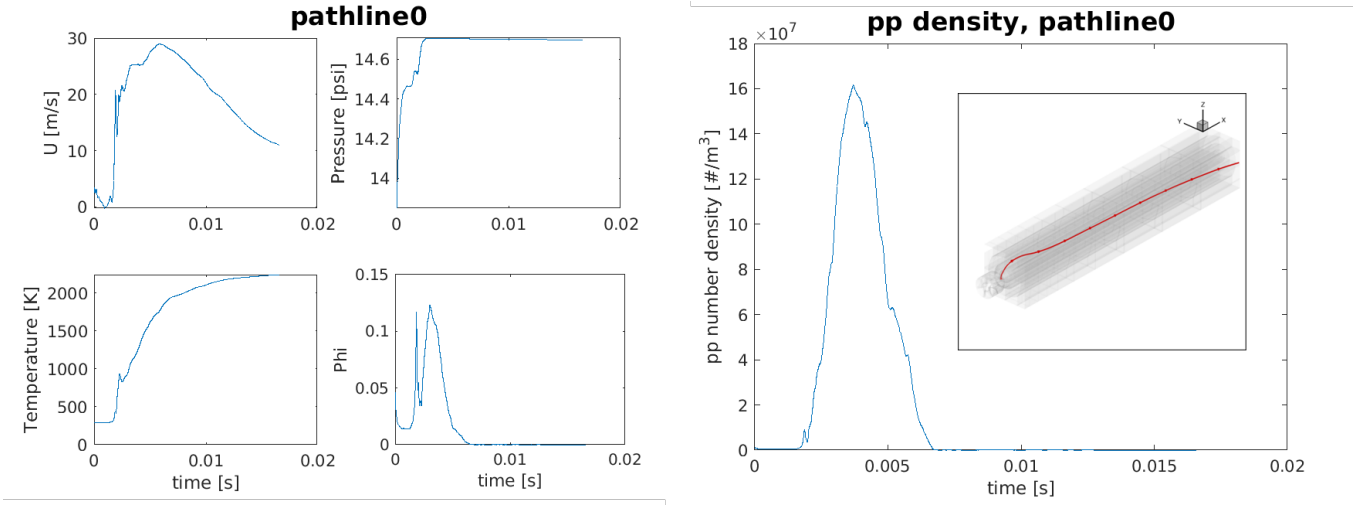

Figure 18. Variation in flow parameters along one path line in the combustor (left) and the calculated primary particle number density, on the basis of classical nucleation theory.

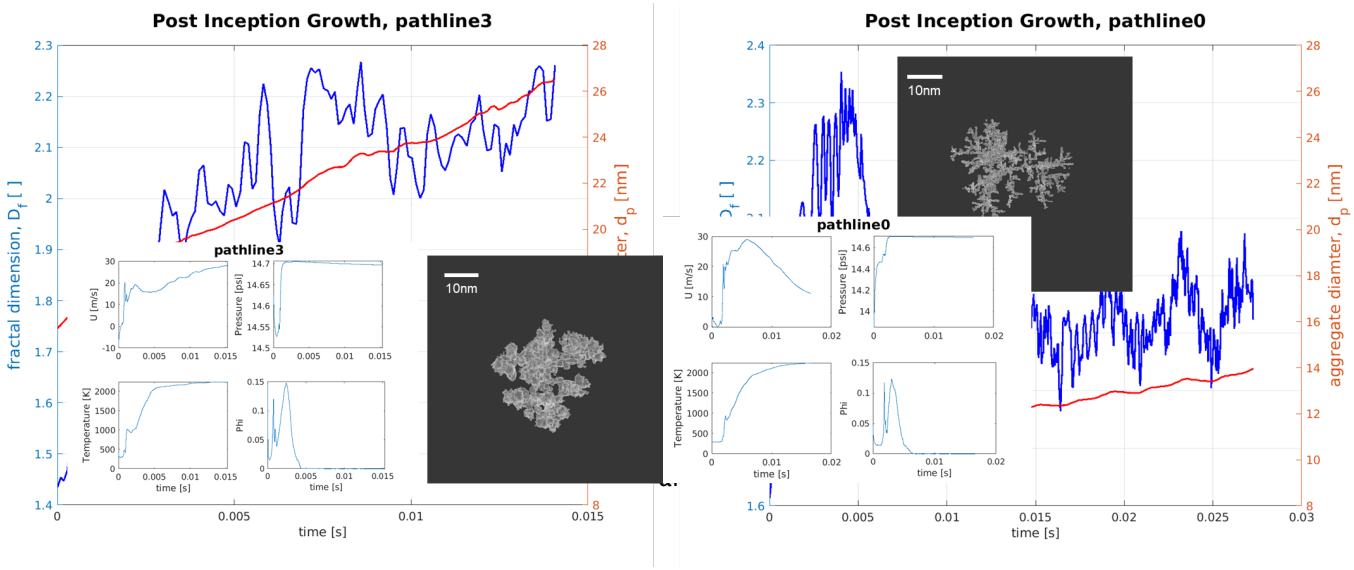

Figure 19. Variation in soot fractal properties along two sample path lines in the combustor.

Milestone
One-way coupled MC studies of surface growth are planned for 9/30/2024.

Major Accomplishments
One-way coupled demonstration of LDI LES data has been used for soot fractal growth.

Publications
None.

Outreach Efforts
None.

Awards
None.

Student Involvement
None.

Plans for Next Period
The future work for the remainder of the project will use actual LES data for the RQL combustor and conduct soot fractal evolution along its path lines, as demonstrated above.

Task 4 – Large Eddy Simulation
GT

Objective
The objective of this task is to develop a physics-informed LES framework to model soot formation in turbulent reacting configurations of canonical configurations and combustors with practical relevance. In the most recent annual efforts, we demonstrated LES-MOMIC coupling for soot evolution in canonical premixed and non-premixed configurations. The current report discusses the LEM-MOMIC framework to address small-scale effects of turbulence-chemistry-soot

interactions on sooting premixed flames. The second part of the report discusses the multiphysics reacting flow simulations inside the RQL combustor at realistic conditions, to provide relevant inputs to collaborating partners.

Research Approach

LES studies of turbulent sooting problems are very difficult because of the multiscale nature of soot inception, coagulation, and surface growth that must be modeled in a highly turbulent and reactive environment, typically in a complex combustor. Most prior studies have focused on global models that approximate small-scale physics. Consequently, many available models account for the underlying physics. In contrast, simulations require some approximations, because the computational resources will never meet the simulation requirements. In the current effort, we balance contributing to the prediction of soot formation physics in a realistic gas turbine combustor with the need to obtain high-fidelity, reliable predictions by using advanced models. To achieve this goal, we leverage our past LES capability and upgrade the models by using the results from MD and MC studies. Soot evolution is tracked with MOMIC, wherein the first six moments of the particle size distribution function are used.

The full set of compressible reacting multispecies Navier–Stokes equations cannot be solved directly, because a direct numerical simulation is not feasible for practical applications. For LES, the large-scale flow features are resolved, and subgrid modeling is used for the smaller scales.

The LES governing equations can be written as follows:

$$\frac{\partial \bar{\rho}}{\partial t} + \frac{\partial}{\partial x_i}(\bar{\rho}\,\widetilde{u_i}) = 0$$

$$\frac{\partial}{\partial t}(\bar{\rho}\,\widetilde{u_i}) + \frac{\partial}{\partial x_j}\left(\bar{\rho}\,\widetilde{u_i}\,\widetilde{u_j} + \bar{P}\,\delta_{ij} - \overline{\tau_{ij}} + \tau_{ij}^{sgs}\right) = 0$$

$$\frac{\partial}{\partial t}\left(\bar{\rho}\,\tilde{E}\right) + \frac{\partial}{\partial x_j}\left[\left(\bar{\rho}\,\tilde{E} + \bar{P}\right)\widetilde{u_i} + \overline{q_i} - \widetilde{u_j}\,\overline{\tau_{ij}} + H_i^{sgs} + \sigma_i^{sgs}\right] = 0$$

$$\frac{\partial}{\partial t}\left(\bar{\rho}\,\widetilde{Y_k}\right) + \frac{\partial}{\partial x_j}\left[\bar{\rho}\,\widetilde{Y_k}\,\widetilde{u_j} - \bar{\rho}\,\overline{D_k}\,\frac{\partial \widetilde{Y_k}}{\partial x_j} + \Phi_{j,k}^{sgs} + \Theta_{jk}^{sgs}\right] = \bar{\rho}\,\widetilde{\dot{w}_k}$$

$$\frac{\partial}{\partial t}\left(\bar{\rho}\,\tilde{Y}_{soot}\right) + \frac{\partial}{\partial x_j}\left[\bar{\rho}\,\tilde{Y}_{soot}\,\widetilde{u_j} - \bar{\rho}\,\overline{D}_{soot}\,\frac{\partial \tilde{Y}_{soot}}{\partial x_j} + \widetilde{V_T}_{soot}\,\tilde{Y}_{soot} + \Phi_{j,k,soot}^{sgs} + \Theta_{jk,soot}^{sgs}\right] = \bar{\rho}\,\tilde{\dot{w}}_{soot}$$

$$\frac{\partial}{\partial t}\left(\bar{\rho}\,\widetilde{M_k}\right) + \frac{\partial}{\partial x_j}\left[\bar{\rho}\,\widetilde{M_k}\,\widetilde{u_j} - \bar{\rho}\,\overline{D}_{soot}\,\frac{\partial \widetilde{M_k}}{\partial x_j} + \widetilde{V_T}\,\widetilde{M_k} + \Psi_{j,k}^{sgs} + \Omega_{j,k}^{sgs}\right] = \bar{\rho}\,\widetilde{\dot{M}_k}$$

Here, $\widetilde{u_i}$ is the *i*-th filtered velocity, $\bar{\rho}$ is the filtered density, and $\bar{P}$ is the filtered pressure, which is computed from the filtered equation of state. $\tilde{T}$ is the filtered temperature, $\tilde{E}$ is the filtered energy, $\widetilde{Y_k}$ and $\widetilde{Y}_{soot}$ represent the filtered *k*-th gas-phase species and soot mass fraction, respectively, and $\widetilde{M_k}$ represents the *k*-th moments of the particle size distribution function. The details regarding the computations of all these quantities have been described elsewhere (El-Asrag & Menon, 2009) and hence are not discussed herein in specific detail. The filtered heat flux $\bar{q}$ can be supplied to an optically thin radiation model to include effects of radiation. The terms $\tau_{ij}^{sgs}, H_i^{sgs}, \sigma_i^{sgs}, \Phi_{j,k}^{sgs}, \Theta_{j,k}^{sgs}, \Psi_{j,k}^{sgs}$, and $\Omega_{j,k}^{sgs}$ contain the effects of the subgrid scale on the filtered quantities. Modeling of these terms remains challenging; in addition, the closed system of equations must be solved together in three-dimensional space with temporal accuracy.

In this work, an eddy viscosity type subgrid model with constant coefficients is used to obtain the closure of subgrid momentum stresses and subgrid enthalpy flux. For the subgrid turbulence chemistry soot interactions, the code is equipped with a multiscale LEM based closure model, partially stirred reactor model, laminar chemistry approximations, etc. In the LEM formulation, the gas-phase species conservation equations are not spatially filtered as in other LES equations. Instead, the exact unfiltered equations are solved by using a two-scale, two-step Eulerian–Lagrangian approach. First, within each LES cell, the one-dimensional LEM model is used to solve for the scalar fields (species mass fraction, soot mass fraction, LEM temperature, and soot integer moments) along a notional line oriented along the maximum scalar gradient. Second, the subgrid scale fields are convected across the LES cell faces by using a Lagrangian transport approach through the splicing algorithm, which reproduces the effect of large-scale advection of the scalars by the flow field. The resulting scalar fields are then filtered in each LES cell to recover LES-resolved species mass fractions to be used in LES-resolved energy and state equations. In Year 3, we first demonstrated the subgrid LEM–MOMIC for the application of the soot MOMIC model within a linear eddy model for turbulence effects on soot formation and growth. The first results

pertaining to these studies are presented. We also conducted LES of the RQL combustor currently being investigated under FAA Project 70, which remains underway. These results are discussed at the end. The data based on these simulations are used by collaborating partners to fine-tune their models, which will be provided to GT.

In the first part of our annual efforts, we focused on implementing the MOMIC model in the standalone LEM to exploit its benefits in studying the effects of small-scale subgrid turbulence on premixed jet flames at two rich equivalence ratios as well as different turbulence Reynolds numbers. These results were presented at the 75th American Physical Society's Division of Fluid Dynamics Meeting in November 2022. The details of the MOMIC model with PAH kinetics and corresponding source terms have been discussed in prior annual efforts and hence are not repeated for brevity. In summary, the current MOMIC model is based on six moments of soot particle size distribution function and an assumption of nucleation based on pyrene dimerization. The surface growth is assumed to occur via hydrogen abstraction carbon addition mechanism. The source terms also include the soot mass growth due to condensation of PAH molecules on the surface of soot particles. The coagulation and aggregation are treated as originally described in the original MOMIC (Frenklach, 2002) approach.

LEM (El-Asrag & Menon, 2009) has been used as a subgrid model for turbulence-chemistry closure inside the LES grid, to capture effects of scales smaller than the LES resolution. Here, we use LEM as a standalone model, which has previously been used to simulate high-Karlovitz-number non-sooting turbulent flames (Sreenivasan and Menon, 2014). The LEM solves temperature evolution and species evolution through a reaction-diffusion equation as well as the MOMIC equations. The turbulent effects are modeled with the triplet mapping procedure, which rearranges the scalar field by the motion of an eddy. This approach has been shown to reproduce the turbulent diffusion associated with high-Reynolds-number inertial range turbulence. The evolution of the scalar field within the LEM domain is shown in Figure 20.

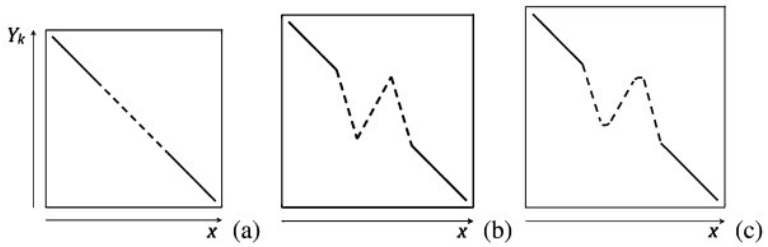

Figure 20. Evolution of the scalar field within the LEM domain.(a) Initial scalar field; (b) After triplet mapping; (c) After reaction-diffusion.

The eddy size (l) is chosen from a turbulent PDF $f(l)$

$$f(l) = \frac{\frac{5}{3} l^{-\frac{8}{3}}}{\left(\eta_e^{-\frac{5}{3}} - l_o^{-\frac{5}{3}}\right)} \quad where \;\; \eta_e = N_n l_o Re^{-\frac{3}{4}}$$

The frequency of the stirring operations is estimated as

$$\lambda = \frac{54}{5}\left(\frac{\nu Re}{c_\lambda l_o^3}\right)\left[\frac{\left(\left(\frac{l_0}{\eta}\right)^{\frac{5}{3}} - 1\right)}{1 - \left(\frac{\eta_e}{l_0}\right)^{\frac{4}{3}}}\right]$$

where η_e is the Kolmogorov length scale, l_o is the integral length scale, Re_t is the turbulent Reynolds number, and c_λ, N_n are the model constants. On the basis of the above two parameters, the eddy location is randomly selected from the permissible locations in the domain. The reaction, diffusion, and stirring operations are mathematically represented as

$$\frac{\partial Y_k}{\partial t} = F_{k,stir} \quad - \frac{1}{\rho}\frac{\partial}{\partial s}(\rho Y_k V_k) + \frac{\dot{\omega_k} W_k}{\rho} \qquad k = 1, \ldots,$$

$$\frac{\partial T}{\partial t} = F_{T,stir} - \frac{1}{\bar{c_p}} \Sigma_{k=1}^{N} c_{p,k} Y_k V_k \frac{\partial T}{\partial s} + \frac{1}{\rho\, \bar{c_p}} \frac{\partial}{\partial s}\left(\bar{\kappa}\frac{\partial T}{\partial s}\right) - \frac{1}{\rho\, \bar{c_p}} \Sigma_{k=1}^{N}(h_k\, \dot{\omega}_k\, W_k)$$

$$\frac{\partial M_r}{\partial t} = F_{M_r,stir} + \dot{\omega}_{M_r} \qquad r = 0,1,2,3,4,5$$

Here, ρ represents the two-phase density, $\dot{\omega}_{M_r}$ denotes the source terms for moments of soot PSDF, N_g denotes the total number of gas-phase species, $F_{k,\,stir}$ is the term for stirring for the species mass fraction, M_r represents the moments of soot PSDF, $F_{M_r,stirr}$ is the stirring for moment terms, Y_k, h_k, ω_k represent the mass fraction, enthalpy, and reaction rate of the k_{th} species, and, $W_k, C_{p,k}\, V_k$ denote the k_{th} species molecular weight, specific heat at constant pressure, and diffusion velocity.

In the current quarterly effort, laminar premixed flames of jet fuel (POSF10325), also commonly known as catA2 in the literature, are conducted with a standalone LEM-MOMIC method. The chemistry is integrated implicitly by using the 62 species reduced jet fuel model (Wang et. al., 2018), in which the length of the domain is 25 mm, and the smallest grid size is 1 μm. The laminar flame properties, such as flame thickness ($\boldsymbol{\delta^o_{L,max}} = \frac{\nu}{S_l^o}$) and flame speed ($\boldsymbol{S_l^o}$), are provided in Table 1.

The turbulent cases simulated with LEM-MOMIC are given in Table 2.

Table 1. Laminar flame properties of Jet A fuel.

$\boldsymbol{\phi}$	$\boldsymbol{S_L^o}$ (m/s)	$\boldsymbol{\delta^o_{L,max}}$ (mm)	$\boldsymbol{\delta_T^0}$ (mm)
1.8	0.227	0.179	0.957
2.0	0.164	0.243	1.18

Table 2. Simulation parameters at various turbulent conditions.

Case	$\boldsymbol{\phi}$	$\frac{\boldsymbol{u'}}{\boldsymbol{S_L}}$	$\boldsymbol{Re_t}$	$\boldsymbol{l_o}$ (mm)	$\boldsymbol{\eta}$ ($\boldsymbol{\mu}$m)	Ka
1A	1.8	10	83	2.0	72.8	9.46
1B	1.8	25	200	2.0	36.3	38.36
2A	2.0	10	83	1.9	91.1	11.02
2B	2.0	25	200	1.9	45.4	43.57

In Table 2, l_o represents the integral length scale, u' denotes the turbulence intensity, the turbulent Reynolds number is defined as $Re_t = \frac{u' l_o}{\nu}$, the Kolmogorov length scale is estimated as $\eta \sim l_o Re_t^{-\frac{3}{4}}$, and the Karlovitz number is calculated as $Ka = \sqrt{\frac{\left(\frac{u'}{S_l^o}\right)^3 \delta_L^o}{l_o}}$. Because LEM-MOMIC is a stochastic model, the statistical averages over the 10,000 instantaneous snapshots are taken to obtain averaged flame profiles. Figure 21 shows how the structure of the flame changes because of isotropic one-dimensional model turbulence, by tracking the temperature profiles. The thickening of the flame with increasing Karlovitz number is observed.

The main aim of the current work is to understand the effects of turbulence due to different equivalence ratios as well as different turbulent conditions. Figure 22 shows how the spatial variations in soot volume fraction and number density profiles occur. As expected, the rich flame shows more sooting behavior. For example, at $\phi = 2.0$, the soot volume fraction levels are roughly four times more than those at $\phi = 1.8$. A similar effect is also observed on the soot number density profiles. The turbulence also appears to profoundly affect the emissions levels. With increasing turbulence, the levels as well as the initiation of soot formation appear to be affected. For example, at $\phi = 1.8$, the maximum soot volume fraction rises from 0.015 ppm to 0.025 ppm. Similarly, the initiation of soot inception also occurs earlier with increasing turbulence. The temperature profile suggests that the preheat zone thickens with increasing Re_t, and hence pyrene formation and soot inception due to pyrene (A_4) occur earlier.

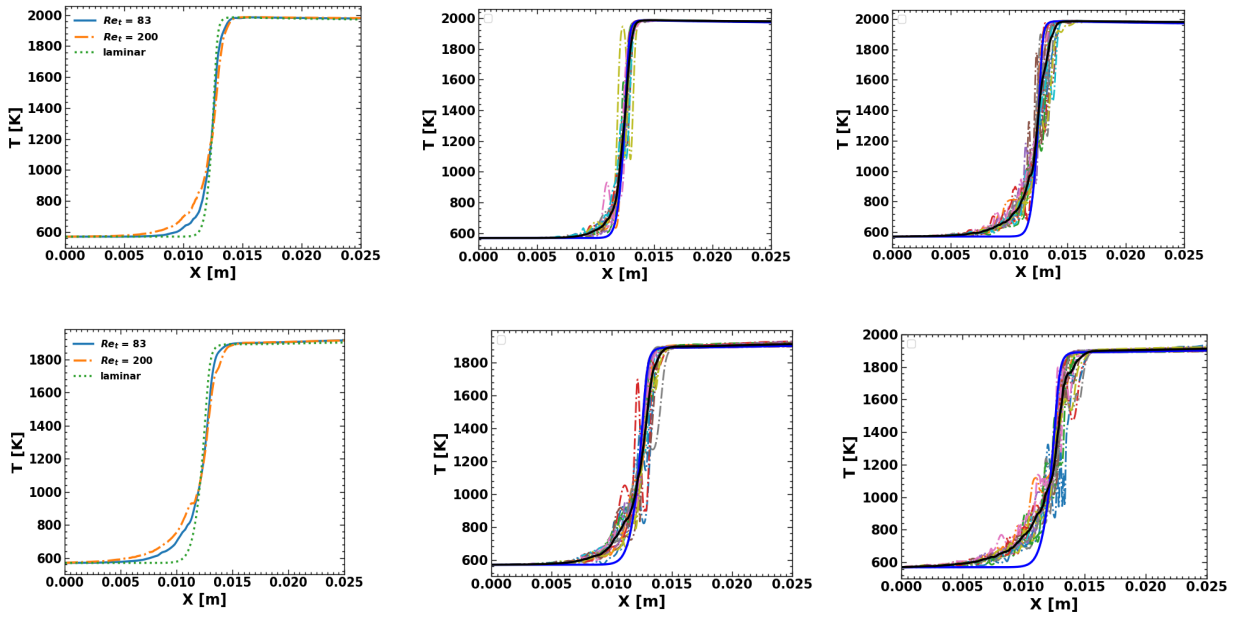

Figure 21. (a) Averaged profiles of temperature at laminar conditions, Re_t = 83 and Re_t = 200. (b) Representative instantaneous snapshots of temperature demonstrating action of eddies at Re_t = 83. (c) Representative instantaneous snapshots of temperature demonstrating action of eddies at Re_t = 200. The top three figures present results for $\phi = 1.8$, whereas the bottom three figures show results for $\phi = 2.0$.

To understand the physics of soot formation with the MOMIC model, we examined the various source terms due to nucleation, coagulation, and surface growth, normalized by their maximum values, to identify their locations of dominance behind the flame. The comparison of their locations is provided in Figures 23–25. The plot shows the competition among nucleation, coagulation, and surface growth zones behind the flame in laminar and turbulent conditions. All these profiles are statistically averaged for stochastic comparison. The coagulation zone closely follows the nucleation zone. The combined effect of surface growth and oxidation is more dominant after nucleation.

The comparison of nucleation and surface growth terms is shown in Figures 23–25 for $\phi = 1.8$. The surface growth adds more soot mass than observed with nucleation under laminar as well as turbulent conditions. The surface growth source terms are further analyzed to understand contributions from surface growth due to C_2H_2 addition and surface oxidation due to O_2 and OH, and are shown in Figure 19 for $\phi = 1.8$. The soot mass addition due to C_2H_2 is almost three times more dominant than O_2 and OH radicals. The oxidation by OH molecules is four times higher than the O_2 molecules.

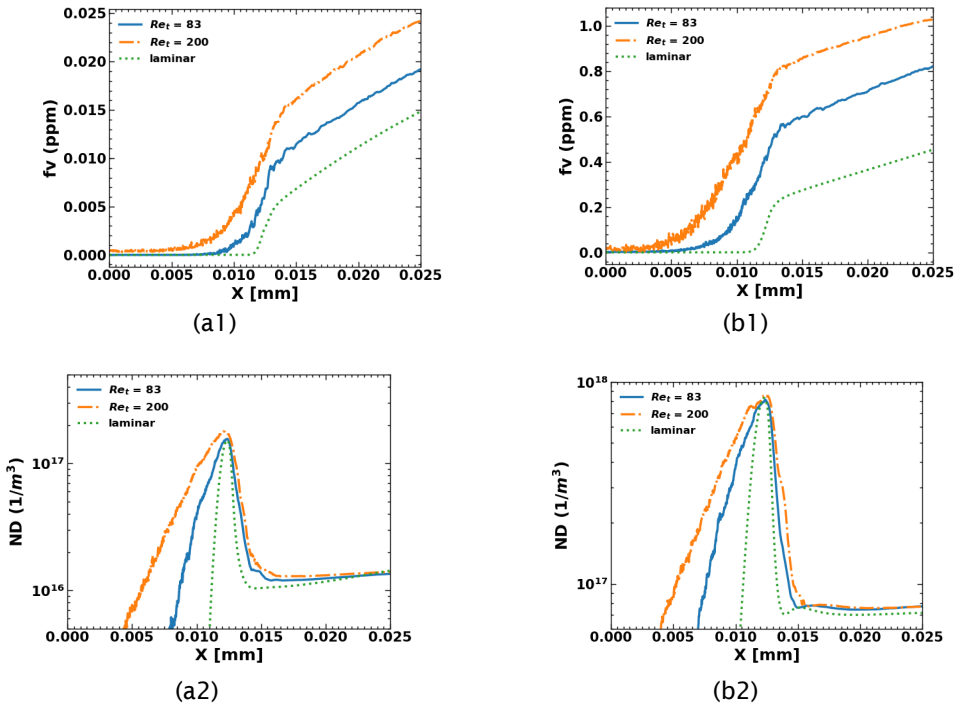

Figure 22. Comparison of the soot volume fraction at laminar and turbulent conditions for (a1) and (a2). Comparison of soot number density at laminar and turbulent conditions for (b1) and (b2).

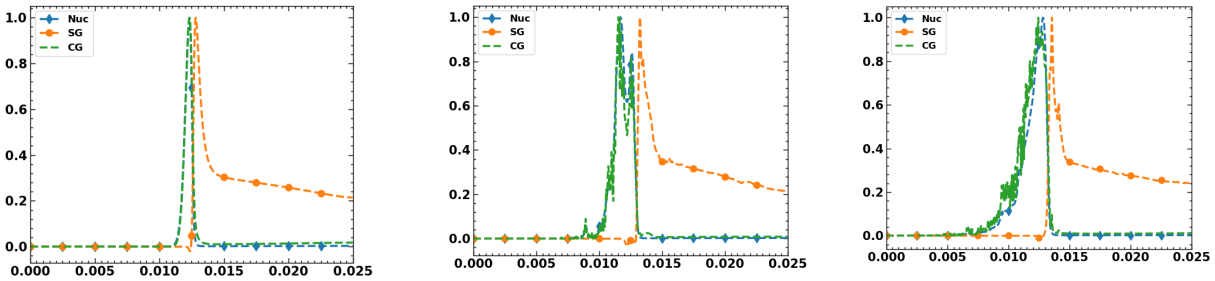

Figure 23. Normalized nucleation (Nuc), coagulation (CG), and surface growth (SG) source terms.

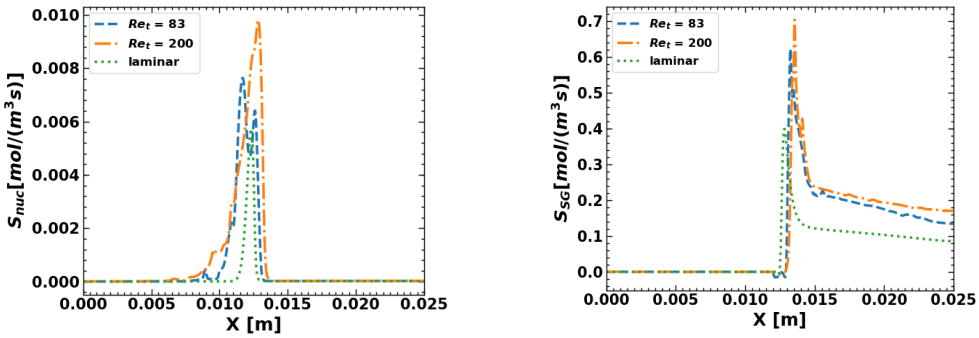

Figure 24. Comparison of the contributions from nucleation and surface growth to soot overall soot growth.

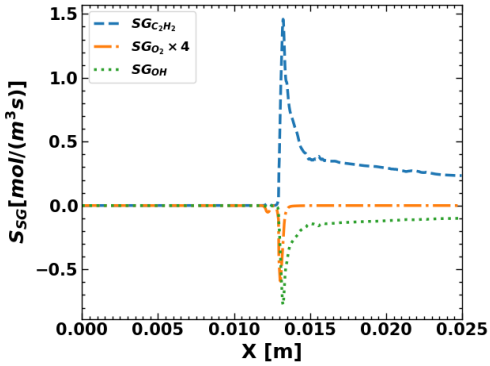

Figure 25. Comparison of the contributions from C_2H_2, O_2, and OH to soot surface growth and oxidation.

In summary, in the first quarter of this annual report, we focused on improving our multiscale LEM model to include soot formation and growth effects due to PAH kinetics. In the remainder of this report, we will discuss LES work conducted to perform large-scale simulations inside an RQL combustor.

RQL combustor

The computer-aided design (CAD) model of the realistic LES rig in the Year 3 effort is shown in Figure 26(a). The RQL burner simulated in GT is a subsection (only one swirler) and is represented in Figure 26(b).

In summary, the entire CAD model consists of an inlet planum, a radial swirler, and eight dilution jets at the top and bottom. As is evident from the three-sector rig, some portions of the top wall and all side walls have glass window panels for the experimental measurements and hence are treated as adiabatic in the current study. Effusion boundary conditions are applied to all remaining walls where glass windows are not present. The side jets near the side walls are difficult to resolve and hence are replaced by a continuous slot for air injection.

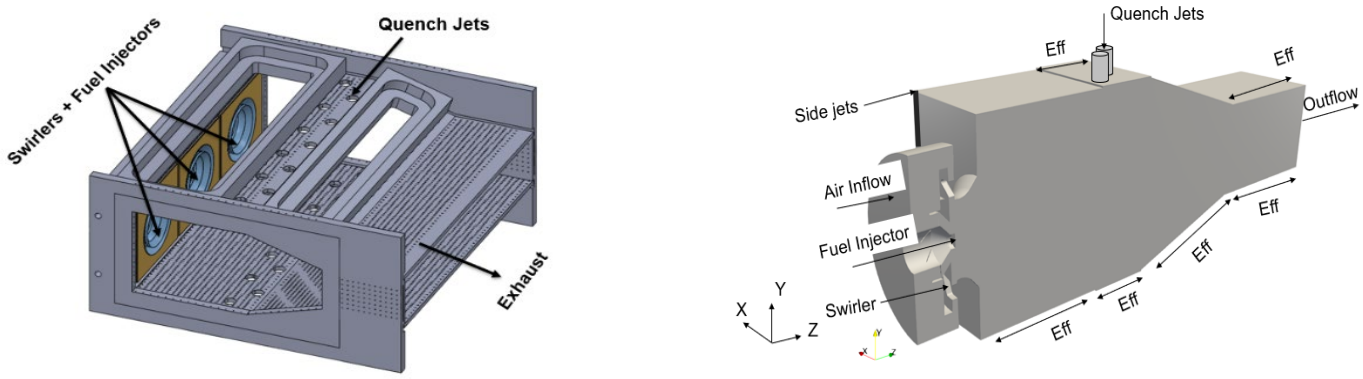

(a) Three-swirler RQL experimental rig (b) Model single-injector combustor

Figure 26. CAD model for the RQL rig.

The entire geometry is split among 5,250 blocks for parallelization. The LES solver is MPI-parallel, and the simulations are run on 1,440 cores. Simulations are conducted on GT's supercomputing cluster (PACE Phoenix) with Intel Ivy-bridge i7 processors. More details regarding the use of LESLIE for simulating turbulent reacting and non-reacting flows inside a gas turbine engine can be found in Panchal (2022). For the model combustor, we are using the practical conditions as initially specified by Honeywell. The inflow air is preheated at T_{in} = 600 K and P_{in} = 5.8 atm, and enters the model combustor through primary swirlers, side jets, effusion holes, and quench jets. The overall total mass flow rate is 0.2785 kg/s and is split as shown in the following Table 3. The fuel mass flow rate is such that the equivalence ratio (ϕ) in the primary zone is 1.8.

Table 3. Mass flow rate split among various components.

Component	Primary swirler	Quench jets	Side jets	Effusion	Fuel	Total
$\dot{m}_{\frac{kg}{s}}$	0.0557	0.1403	0.0278	0.0547	0.00679	0.2854
Split %	19.52	49.16	9.75	19.18	2.39	100

A fully compressible Eulerian finite volume formulation for the gas phase is used. An eddy viscosity approach with a one-equation subgrid kinetic energy (k_{sgs}) model is used for the closure of gas-phase subgrid scale fluxes. A well-established multiblock structured fully compressible finite volume solver, LESLIE, is used for simulation with a hybrid second-order central and third-order upwind method. A fourth-order Runge–Kutta solver is used for solving the Lagrangian equations. The dilute injection of spray is the current focus. For computational efficiency, instead of tracking of individual Lagrangian particles, the particles are grouped in parcels, and the parcels are tracked in a Lagrangian manner. A particle-per-parcel value of 8 is used in this work and has been shown to provide a good balance between accuracy and efficiency for gas-turbine combustor LES. The inflow boundary condition is modeled by using a characteristic Navier–Stokes boundary condition. The outflow is modeled by using a sponge boundary condition. The liquid fuel droplets are injected through hollow cone injector and have a log-normal distribution for sizes with a Sauter mean diameter of 36 μm. A breakup model is not considered in this work, because the droplets are assumed to have a smaller Sauter mean diameter. However, for larger droplets, the code can handle secondary breakup, if needed. A globally reduced six-species two-step KERO-BFER mechanism (Franzelli, 2008) is used to represent the finite rate chemistry effects.

The time step for the reacting flow simulations is 9.4×10^{-9} s. First, we collected traces (temporal history between 40 ms and 52 ms) of mass flow rates to verify if boundary conditions are correctly applied as shown in Figure 27. It suggests that the mass flow rate at outflow is equal to the summed mass flow rate at all inflow boundaries and conserves mass, thus ensuring that the mass flow rates at each boundary do not substantially oscillate.

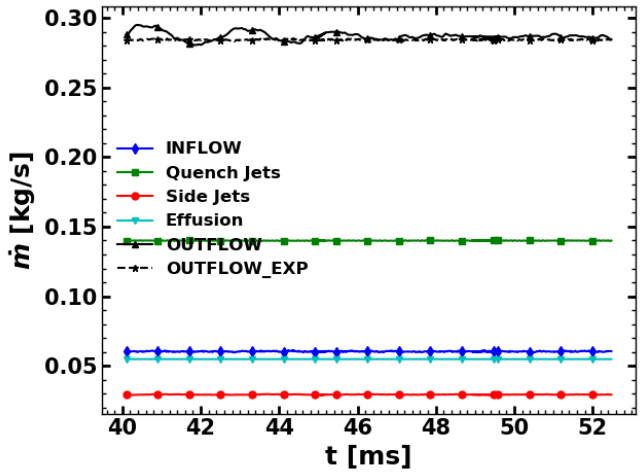

Figure 27. Temporal history of surface averaged mass flow rate at boundaries of the combustor.

Initially, statistically averaged flow features of non-reacting flow field are shown in Figure 28. As a result of the swirl, a low-pressure zone is created in the center, forming a vortex breakdown bubble (VBB) (also known as the central recirculation zone)—a key feature of swirling flows. A negative velocity is observed in the center, as shown by the axial velocity contour in Figure 28(a), and also observed in statistically averaged axial velocity along the height at various axial locations, which are shown via line plots in Figure 28(b). The initial lines between (z/L < 0.2) show the negative axial velocity in the line plots. In a typical turbulent reacting swirling flow, the hot products are trapped inside the VBB and provide necessary high temperatures for vaporization of the droplets, which react after mixing with the oxidizer.

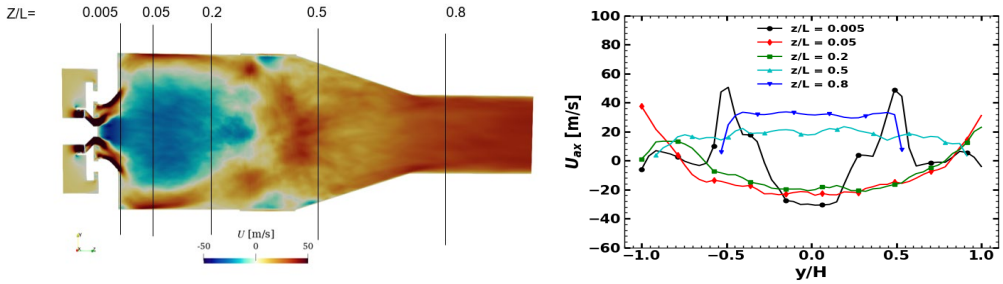

(a) Time averaged axial velocity contour (b) Axial velocity variation along the height

Figure 28. Representative axial velocity field through the center of the combustor.

The shape of this VBB is shown in Figure 29(a), by identifying the iso-surface of velocity where axial velocity is zero. The line plot of averaged axial velocity (Figure 27(b)) along the length of the combustor is also shown via line plots at two locations along the x axis (x/L_x = 0.5 represents the center of the combustor, and x/L_x = 0.345 represents the center of one of the dilution jets). The line plots suggest that the overall length of the recirculation zone is one third the length of the overall combustor.

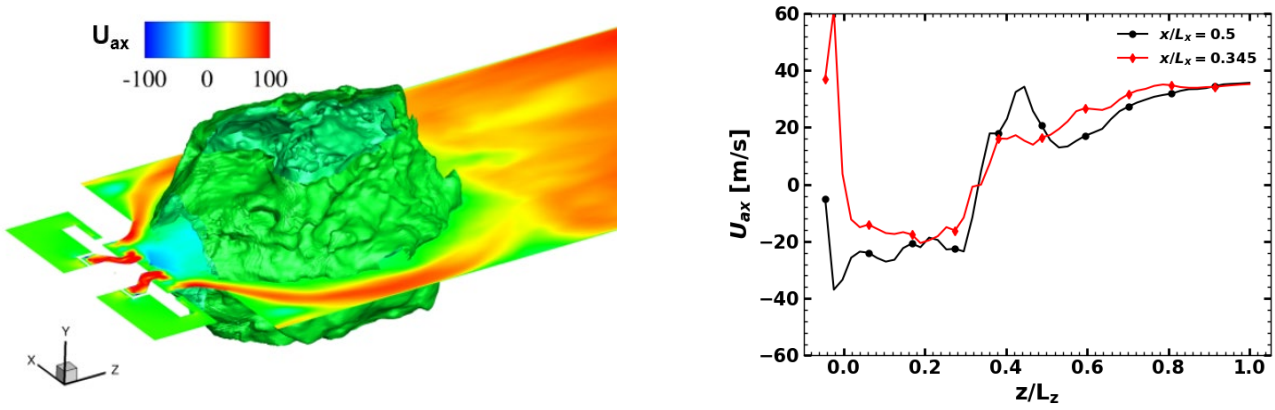

(a) VBB iso-surface

(b) Axial velocity along the axial length

Figure 29. VBB features of the swirling flow inside the combustor.

Kerosene droplets are injected from the center of the injector, and an initial hotspot is superimposed on the non-reacting flow field to kickstart the reacting flow. The simulations are run until the flame is fully stable. The instantaneous features of temperature field, and major product species (CO_2 and H_2O) are shown in Figure 30 along the vertical and horizontal planes of the combustor in the snapshots below. A lifted flame anchored near the injectors is observed. The incoming fuel droplets vaporize because of high temperature, mix with the surrounding oxidizer, and burn at a high temperature of approximately 2500 K. As evident from the field, particularly in Figure 30(a), the cold quench jets of air enter the combustor from the top and bottom, and quench the flame; consequently, a low-temperature zone is observed in the second half of the combustor. The cooling jets mix with the products, and a highly turbulent mixing is observed, as is characteristic of RQL combustor. The primary zone contains most of the product species and is diluted by the incoming air through quench jets, as indicated in Figure 30(b) and Figure 30(c).

In summary, the current efforts have established the reacting flow inside a model RQL combustor at realistic conditions closer to actual test conditions. Stable reacting flow simulations are conducted, wherein the global equivalence ratio is rich in the primary zone, as in an RQL combustor. Because globally reduced six-species kerosene kinetics is used to perform these simulations, information for species relevant to soot formation and growth cannot be obtained; this challenge is the focus of continuing effort. In the future, we will focus on using the reduced global kinetics (with PAH) and the optimized soot kinetics developed by RTRC to study soot formation and growth from the RQL combustor. In parallel, we will also provide the current reacting flow data to RTRC for one-way coupled MC simulations that can provide more information regarding the tendency of soot to form characteristic aggregate structures; moreover, a more realistic fractal dimensions of soot particles at tabulated background conditions will be used within the LES code.

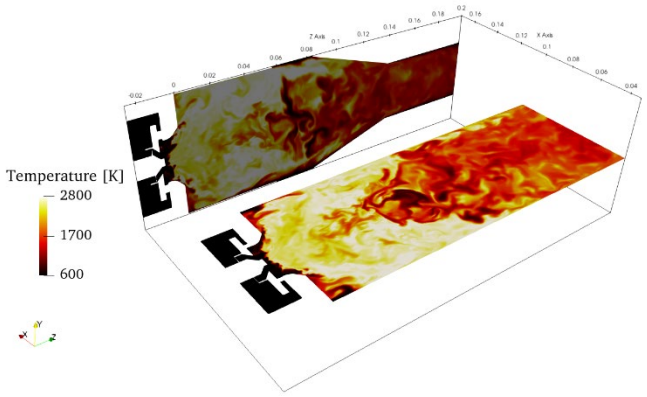

(a) Temperature inside the combustor

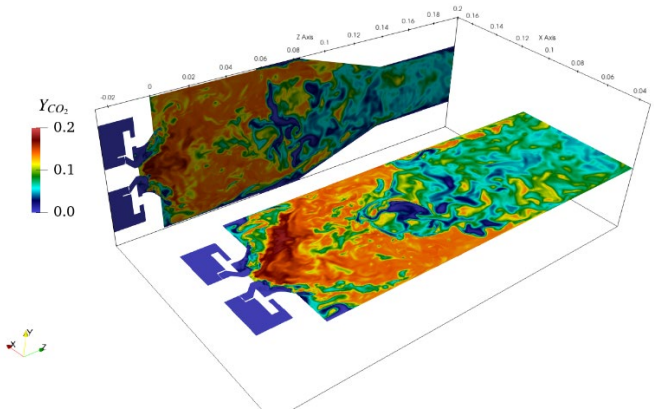

(b) CO_2 mass fraction

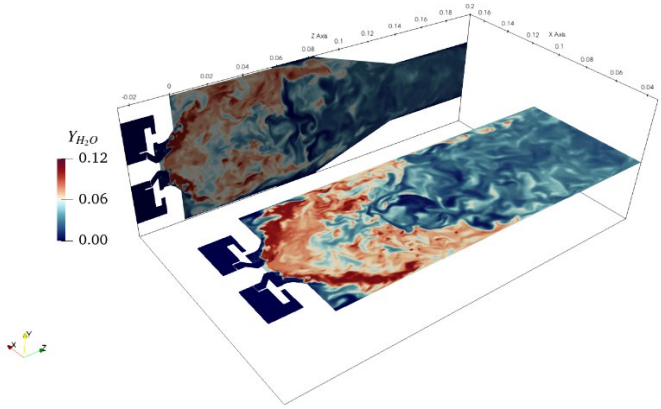

(c) H_2O mass fraction

Figure 30. Instantaneous features of temperature, CO_2 mass fraction, and H_2O mass fractions along the horizontal and vertical mid-planes of the combustor.

Milestones
LEM-MOMIC model coupling for turbulence-soot-chemistry interaction and LES of a practical RQL combustor are planned for 9/30/2024

Major Accomplishments
Efforts focused on soot-turbulence-chemistry interactions on canonical turbulent premixed flames and LES of multiphysics flow inside the RQL combustor being investigated under Project 70.

Publications
None.

Outreach Efforts
None.

Awards
None.

Student Involvement

PhD student Shubham Karpe has been assisting in the development of the MOMIC framework within the LES code at GT.

Plans for Next Period

The future work at GT involves incorporating inputs from the partner groups into the MOMIC model at GT. We will also conduct RQL simulations at these conditions with the improved soot model, to provide a final demonstration of the model.

References

Balthasar, M., & Frenklach, M. (2005). Monte-Carlo simulation of soot particle coagulation and aggregation: the effect of a realistic size distribution. *Proceedings of the Combustion Institute, 30*(1), 1467–1475. https://doi.org/10.1016/j.proci.2004.07.035

Chen, J.-Y. (1988). A general procedure for constructing reduced reaction mechanisms with given independent relations. *Combustion Science and Technology*, *57*(1-3), 89–94. https://doi.org/10.1080/00102208808923945

Colket, M. B., Hall, R. J., & Stouffer, S. D. (2004, June 14-17). *Modeling soot formation in a stirred reactor* [Presentation]. Proceedings of the ASME Turbo Expo 2004: Power for Land, Sea, and Air, Vienna, Austria. https://doi.org/10.1115/GT2004-54001

Glarborg, P., Kee, R. J., Grcar, J. F., & Miller, J. A. (1986). *PSE: a Fortran program for modeling well-stirred reactors* (Report No. SAND86-8209). Sandia National Laboratories, Livermore, CA.

El-Asrag, H., & Menon, S. (2009). Large eddy simulation of soot formation in a turbulent non-premixed jet flame. *Combustion and Flame, 156*(2), 385–395. https://doi.org/10.1016/j.combustflame.2008.09.003

El-Asrag, H., Lu, T., Law, C. K., & Menon, S. (2007). Simulation of soot formation in turbulent premixed flames. *Combustion and Flame, 150*(1-2), 108–126. https://doi.org/10.1016/j.combustflame.2007.01.005

Frenklach, M. (2002). Method of moments with interpolative closure. *Chemical Engineering Science, 57*(12), 2229–2239. https://doi.org/10.1016/s0009-2509(02)00113-6.

Franzelli, B., Riber, E., Sanjosé, M., & Poinsot, T. (2010). A two-step chemical scheme for kerosene–air premixed flames.*Combustion and Flame*, *157*(7), 1364-1373. https://doi.org/10.1016/j.combustflame.2010.03.014

Kireeva, E. D., Popovicheva, O. B., Persiantseva, N. M., Timofeyev, M. A., & Shonija, N. K. (2009). Fractionation analysis of transport engine-generated soot particles with respect to hygroscopicity. *Journal of Atmospheric Chemistry*, *64*(2-3), 129–147. https://doi.org/10.1007/s10874-010-9173-y

Kollrack R., (1977) ASME paper 76-WA/GT-7, Dec.

Langer, R., Mao, Q., & Pitsch, H. (2023). A detailed kinetic model for aromatics formation from small hydrocarbon and gasoline surrogate fuel combustion. Combustion and Flame, 258, 112574. https://doi.org/10.1016/j.combustflame.2022.112574

Leung, K. M., Lindstedt, R. P., & Jones, W. P. (1991). A simplified reaction mechanism for soot formation in nonpremixed flames. *Combustion and Flame, 87*(3-4), 289–305. https://doi.org/10.1016/0010-2180(91)90114-Q

Lu, T., & Law, C. K. (2005). *A directed relation graph method for mechanism reduction.* Proceedings of the Combustion Institute, *30*(1), 1333–1341. https://doi.org/10.1016/j.proci.2004.08.145

Panchal, A., & Menon, S. (2022). Large eddy simulation of fuel sensitivity in a realistic spray combustor II. Lean blowout analysis. *Combustion and Flame*, *240*, 112161https://doi.org/10.1016/j.combustflame.2022.112162

Saldinger, J. C., Elvati, P., & Violi, A. (2021). Stochastic and network analysis of polycyclic aromatic growth in a coflow diffusion flame. *Physical Chemistry Chemical Physics, 23*(7), 4326–4333. https://doi.org/10.1039/d0cp03529g

Srinivasan, S., & Menon, S. (2014). Linear eddy mixing model studies of high Karlovitz number turbulent premixed flames. *Flow, turbulence, and combustion*, *93*, 189-219 https://doi.org/10.1007/S10494-014-9542-8

Stouffer, S., Striebich, R. C., Frayne, C. W., & Zelina, J. (2002, July 12-17). *Combustion Particulates Mitigation Investigation Using a Well-Stirred Reactor* [Presentation]. 38th AIAA/ASME/SAE/ASEE Joint Propulsion Conference & Exhibit, Indianapolis, IN.

Sun, Y., & Beckermann, C. (2007). Sharp interface tracking using the phase-field equation. *Journal of Computational Physics, 220*(2), 626–653. https://doi.org/10.1016/j.jcp.2006.05.025

Wang, H., Xu, R., Wang, K., Bowman, C. T., Hanson, R. K., Davidson, D. F., Brezinsky, K. and Egolfopoulos, F. N. (2018) A physics-based approach to modeling real-fuel combustion chemistry-I. Evidence from experiments, and thermodynamic, chemical kinetic and statistical considerations *Combustion and Flame, 193:502-519* https://doi.org/10.1016/j.combustflame.2018.03.019

Xu, Z., & Meakin, P. (2008). Phase-field modeling of solute precipitation and dissolution. *The Journal of Chemical Physics, 129*(1), 014705. https://doi.org/10.1063/1.2948949